Investigation of the Afterglow in Helium-Xenon Mixtures at High Pressures

H. Zinko and J. Johansson

AB Atomenergi, Studsvik, Fack, Nyköping, Sweden

(Z. Naturforsch. **29 a**, 577–587 [1974]; received October 12, 1973)

The behaviour of high pressure helium afterglows has been measured by means of conductivity and light intensity decay measurements. The plasma was created in a pulsed discharge of typically 30 μsec length and then investigated by means of time resolved spectroscopy and probing pulse diagnostics under conditions which are of interest for noble gas afterglow MHD generators, i. e. a pressure range of 1–4 atm static pressure, the temperature varying from 600–970 °K.

A marked increase in plasma lifetime was found when xenon was seeded with a rate of 10^{-4} to 10^{-3} to helium. This effect is ascribed partly to the influence of Penning ionization and partly to the fact, that slowly recombining atomic xenon ions dominate the recombination behaviour at the lower xenon seed rates during the investigated time interval of 150 μsec. The pressure dependent effective recombination coefficient is found to be $(0.95+1.95\cdot10^{-3}P_0)\ 10^{-8}\,\mathrm{cm^3\,sec^{-1}}$ for pure helium and $(0.2+5.1\cdot10^{-4}P_0)\ 10^{-8}\,\mathrm{cm^3\,sec^{-1}}$ for a xenon seed rate of $3\cdot10^{-4}$ (P_0 = reduced pressure in Torr).

I. Introduction

The noble gas afterglow MHD generator concept (NOGAG), which permits the operation of MHD generators without metallic seed has received increasing attention in the past few years. The reason for this is, that this generator type is expected to operate under working conditions which are comparable to those of Cs-seeded MHD-generators but with the advantage, that no metallic seed has to be applied to and recovered from the closed noble gas loop. The idea was first proposed by Braun [1] as an "unconventional" generator concept in connection with nuclear preionization and has recently obtained increased interest as one serious alternative among others, all aimed at overcoming the physical and technological problem hitherto met in alkali seeded noble gas MHD generators. A preionized noble gas with reasonably long lifetime, e.g. helium is proposed to be used as a working fluid. The helium plasma recombines during its travel through the generator but the ionization is decoupled from the generated current because the induced electric fields are too weak to procedure a sufficient degree of thermal ionization, and therefore no ionization instabilities are expected in such a plasma (Palmgren [2]). Thus a high Hall parameter can be reached and the generator operated in the Hall-mode with the advantage of single-circuit high voltage output.

Reprint requests to H. Zinko, AB Atomenergi, Studsvik, Fack, *S-611 01 Nyköping 1*, Sweden.

Principally the operation of such MHD-generators depends on the following conditions which have to be fulfilled simultaneously in order to render possible a successful power generation: Creation of a plasma uniformly distributed over the channel cross-section, long life-time of the charge carrier and plasma stability in spite of the relatively strong inhomogenity of the electron density and electrical conductivity along the axis and the high magnetic fields.

This paper deals with the second of the mentioned problems, i.e. measurements of the lifetime of He and He-Xe after-glows under conditions of interest in MHD-generators. It is the aim of this report to present experimental data for the plasma lifetime on which performance calculations of NOGAG MHD-generators can be based.

From the study of the literature it becomes evident that the experimental results only at low gas pressures, when He^+ is the dominant ion, are in reasonable agreement with the theory of collisional radiative recombination [3]. When the gas pressure is higher, molecular helium ions are formed, and the recombination processes become more complex. It was recognized that the spectral band emission, associated with bound excited states of the He_2 molecule, is caused by the collisional radiative recombination of He_2^+ ions. The recombination coefficient α was found [4–6] to have one component proportional to the gas density, in the pressure range 10 – 760 Torr, which was interpreted as a three-body recom-

bination of He_2^+ stabilized by neutral helium atoms described by Bates and Khare [7]. Recently, evidence for dissociative recombination of He_2^+ ions for afterglows up to 55 Torr has been found [8–10]. It turns out, that the real recombination coefficient of He_2^+ ions are higher than originally thought and that the low effective recombination coefficients are caused by a strong source of ions in the afterglow probably generated by mutual metastable collisions [6]. Additionally even He_3^+ and He_4^+ ions were found to play a role in high pressure afterglows and to contribute to the pressure dependence of the recombination coefficient [11–13].

In spite of the big effort to illuminate the complex and coupled processes going on in the afterglow, a consistent description for the medium pressure region is still missing. The same holds for plasmas at the very high pressures expected in MHD generators.

Preliminary results for high pressure helium afterglow plasmas were presented at the 5th International Symposium on MHD Power Generation, Munich 1971. Ellis et al. [14] found the highest recombination rates measured in a ionization chamber with ions created by nuclear reactions with only a weak influence of the gas density on the effective recombination coefficient. Zinko et al. [15] found, in a pulsed discharge experiment, recombination rates which were lower by an order of magnitude as compared to those of Ref. [14], but α_{eff} showed a strong density dependence. Finally, Hahn and Salvat [16] measured, in flowing helium which was heated by means of an arc heater, a recombination rate at 1500 °K and 1 atm which agreed very well with that obtained from the Studsvik group [15] under the same gas condition. Zinko et al. [15] reported also that the plasma life-time could be further increased, when a small amount of another noble gas was added to helium. The reason was supposed to be Penning ionization of the seed gas caused by metastable helium ions. Because of the high reaction cross-section, this effect should be mostly marked with xenon as the seed.

In this paper the results measurements during the afterglow of a pulsed high pressure discharge in He-Xe mixtures are reported. In Section II the experimental apparatus and the diagnostic methods are presented, the results are discussed in Section III and summarized in Section IV.

II. Experimental Apparatus and Diagnostic Methods

The experimental set-up was changed compared to that reported in Zinko et al. [15] in order to isolate the discharge space better from the surrounding heating wires.

The new set-up of the electrodes is shown in Figure 1. Molybdenum electrodes of 2.5 mm diameter were used with pointed ends about 7 mm apart. Anode and cathode are isolated by means of quartz tubes. The entire space between electrodes and heating coils was isolated by another T-formed quartz tube of 15 mm inside diameter, large enough to avoid wall diffusion of the charge carrier at pressures above 1 atm. Through the arm of the T-tube spectroscopic measurements could be carried out. In this way, the discharge space was electrically isolated from the heater and particles emitted from the heating coil were prevented from entering the discharge space. The block diagram for the complete experimental equipment is shown in Figure 2.

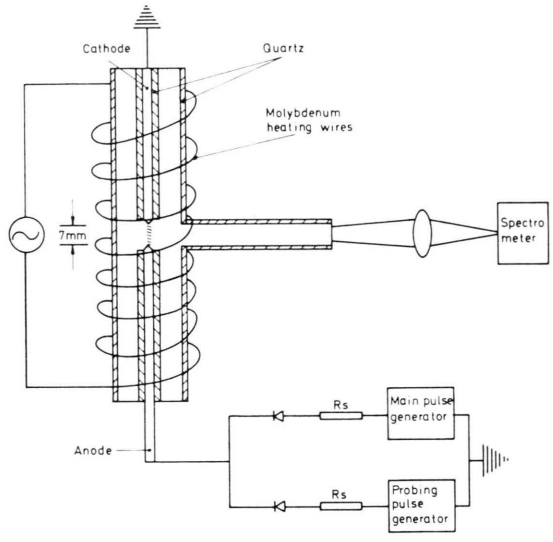

Fig. 1. Final electrode arrangement with the quartz T-tube isolation.

The following experimental procedure was observed. Helium with guaranteed impurity level below 2 ppm was fed from the bottles by a reducer value to the discharge chamber and then through a leak valve to the pump. Before the entrance in the discharge chamber the gas was led through a purification system consisting of a calcium filter, a hopcalite furnace and a cold trap at liquid nitrogen temperatures. The experiment chamber could be evacuated down to 10^{-7} Torr by means of an ion

pump, whereas the rest of the system was kept at a pressure below 10^{-3} Torr for at least 12 hours before starting any experiments. Immediately before

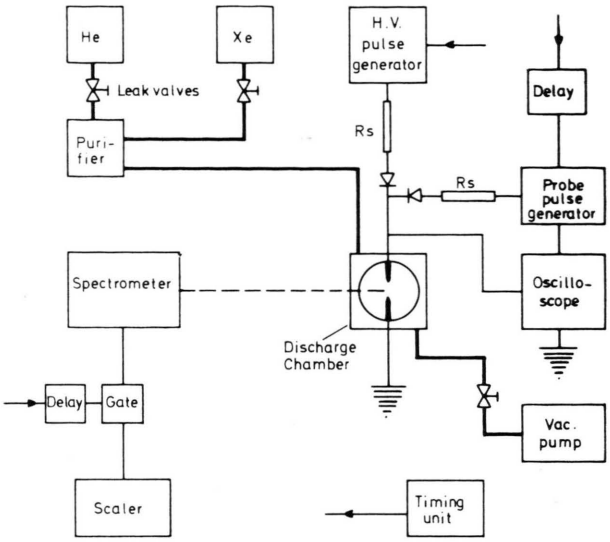

Fig. 2. Block diagram of the experimental set up.

the experiments were carried out, the systems was purget by a heavy helium flow for about 30 minutes. The helium flow rate for each pressure was controlled by the pump leak valve and was calibrated by checking the pressure increase with the leak valve closed. (The volume of the system was known from separate measurements.) Xenon was fed in a similar way to the system but without passing the cold trap. The xenon leak rate was controlled by another leak valve and calibrated by measuring the pressure increase in the range of some millitorr; care was taken to ensure that the pressure difference over the inlet leak valve was the same in all experiments.

The gas purity was spectroscopically checked during the experiments. A weak H_β line about 1% in intensity of the total helium line intensity and also a N_2^+ band-head at 3914 Å of about the same strength as H_β were observed. The impurity level increased slightly at higher temperatures, but was almost constant in time, since the discharge chamber was flushed with a constant gas stream of 0.15 l/sec during the course of the experiment.

In order to reduce emission of metal atoms from the electrodes, the discharge was operated in the glow discharge mode. When transition to an arc occurred, molybdenum lines could be observed in the discharge spectrum, together with an increase in plasma lifetime.

Because any disturbance of the afterglow plasma should be avoided, the temperature was measured with an optical pyrometer. By means of a black hole inside a graphite body, which could be placed between cathode and anode, the temperature produced by the heater was measured in the central region. We calibrated the power fed into the heater as a function of the gas pressure and the helium flow rate. The highest temperature reached was about 970 °K and estimated to be correct within $\pm 50°$. This margin includes also the possible temperature increase which originates from the joule heating under the active discharge.

In principle the measurements are performed in the following manner. A high voltage initiates a pulsed discharge between two molybdenum electrodes in high purity helium flowing through the discharge chamber. After a certain time (typical value 50 μsec) the discharge circuit is interrupted and the resultant afterglow studied with the help of time resolved spectroscopy and with conductivity measurements. For the conductivity measurements a subsidiary probing pulse was applied to the same electrodes over a series resistance after the end of the active discharge and the time dependence of current and voltage in a properly adjusted pair of probes was displayed on a Textronic 556 oscilloscope. The probing pulse could be gated at any time of the afterglow. Care was taken that the probing pulse (5 – 10 Volt) did not influence the ionization degree during the afterglow. However, an applied electric field results in an additional heating of the electrons, which was taken into account when the electron density was calculated (see Section III C). A typical oscilloscope trace is shown in Figure 3. The length of the probing pulse (of the order of 50 – 100 μsec) did not affect the results. The frequency of the pulsed discharge was 100 sec^{-1}. For each discharge the plasma diameter was measured spectroscopically by scanning over the afterglow. Alternatively, line intensity measurements of the afterglow emission in the spectral range between 2500 °Å and 11000 °Å could be performed with the time sampling techniques. An absolutely calibrated Czerny-Turner 1 m-spectrometer was used. The photomultiplier could be gated over the whole interesting region of active discharge and afterglow.

III. Results

From the recorded traces of the electrical probing pulse as shown in Figure 3 only the total plasma resistivity can be directly derived. For calculation of the electrical conductivity, the area of the discharge has to be known according to

$$\langle \sigma \rangle (t) = \frac{U(t) - V(t)}{V(t) - V_e(t)} \frac{l}{A(t)} \frac{1}{R_S} . \qquad (1)$$

$\langle\sigma\rangle$ is an average conductivity of the plasma column, $U(t)$, $V(t)$ and V_e denote the probing e.m.f., the voltage between the electrodes and the electrode drops, all varying in time, $A(t)$ is the discharge area, l the electrode gap and R_S the series resistance. In order to find the mean plasma conductivity it was therefore necessary to measure the discharge profile and the electrode drops separately.

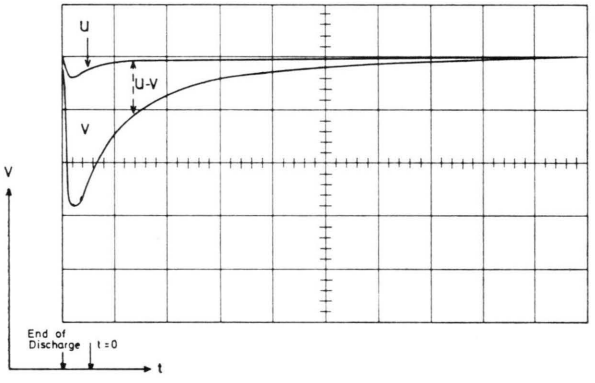

Fig. 3. Typical oscilloscope record for conductivity measurements (U = applied e.m.f., V = voltage between the electrodes, $U-V$ = voltage over series resistance).

A) The Discharge Profile

The time dependent line intensity profile at 5876 Å was measured by scanning across the discharge and calculating the Abel-inversion from the measured profiles. The result is then the actual radial emission profile as shown e.g. in Figure 4 for three different times in the afterglow in pure helium for $p=1$ atm and $T=970\,^{\circ}$K, discharge current $=3.2$ A. It can be seen that there is a tendency for the afterglow plasma to widen with time, but in no case was this expansion more than 15% over the first 150 μsec in the afterglow. The widening of the afterglow was only slightly dependent on the current in the active discharge as it was also on gas temperature and pressure, so the width may be assumed approximately constant. The fact that the maximum radial profile change is only about 15% during the measured time interval, can be taken as a proof that diffusion does not play much part in the loss of the charged particles under the given conditions. Furthermore, the discharge profile may change not only through diffusion processes, but also through volume recombination in a recombination dominated plasma, as Gray and Kerr [17] have shown for a wall-limited discharge. In the case of a self-constricted plasma, which we consider here, the situations is similar, as numerical calculations for a combined diffusion recombination influenced afterglow showed [18].

The diameter was then taken from the intensity profile at $40-50$ μsec in the afterglow and was derived in the following way. The helium atomic line intensity at 5876 Å was assumed to be proportional to a two-body recombination process and therefore $I_{5876} \sim n_e^2$. The n_e profile was determined, and the effective radius R_{eff} of the discharge evaluated by means of the definition

$$2\int_0^R n_e(r)\cdot r\,dr = n_{eA}\,R_{\text{eff}}^2 \qquad (2)$$

(n_{eA} = electron density on the axis, R = radius for which the line emission was 2% of the value on the axis. Equation (2) defines R_{eff} as the radius of an equivalent discharge which has a constant electron density with the same value as the real discharge on the axis (see also Figure 4).

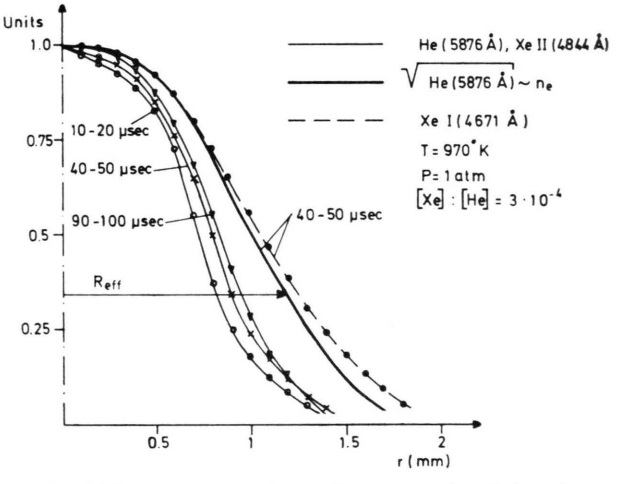

Fig. 4. Abel-inverted experimentally measured radial emission profiles of several lines. The thick full line (n_e) was calculated from the He-5976 Å line ($n_e \sim \sqrt{I_{He}}$).

If a three-body recombination process had been responsible for the emitted light, the effective radius for the case of Figure 4 would be 15% larger resulting in a lower electron density. But there are strong arguments, that the two-body recombination mechanism dominates under the given conditions. The situation was namely changed when xenon was seeded to helium. At a xenon rate of $3\cdot10^{-4}$ cet.par. the helium lines showed about the same profile as in the case without xenon. A similar profile was derived for XeII lines. But the profile of xenon I was

much broader as can be seen from Figure 4. A possible explanation for this is, that the field distribution across the plasma is inhomogeneous due to the pointed electrodes and the relatively small electrode gap, so that the outer region of the discharge is dominated by the atoms with lower lying excitation levels. From the light decay measurements however, which will be discussed below, it can be concluded that the emitted atomic XeI intensity, instead of following a quadratic or cubic relation, is by and large directly proportional to the electron density. Taking the square root of the helium I discharge profile, one gets a profile quite similar to that of xenon I, whereas a n_e profile following the cubic root of the HeI intensity is relatively broad and by no means coincides with the XeI profile. Therefore the effective discharge area was calculated from the square root of the helium 5876 Å line for both cases with and without xenon seed.

B) The Electrode Voltage Drops

In order to obtain a correct value for the electrical conductivity, the electric field and the current density have to be measured. The latter was done by dividing the total probing pulse current by the area derived using the procedure described above. The electric field of the probing pulse could not be measured at the same time as the afterglow measurements were carried out, but it could be derived from the applied probing pulse voltage and the electrode gap width, when the electrode drops were known. Therefore separate measurements of the electric fields of the probing pulse were performed by means of double probes in a larger electrode gap (20 mm) but under the same plasma conditions. Two 0.25 mm diameter molybdenum electrodes were inserted, at distances of 1 mm from the anode and cathode, respectively. Comparison of the product of the measured electric field times the electrode gap width with the applied voltage resulted in a difference called "effective electrode drop" which is shown in Figure 5 for two probing voltages (5 and 10 Volt). The electrode drops increased slightly with increasing probing current, but it is easy to see that its absolute value lies around 1 Volt. Thus 1 Volt electrode drop was included when the electrical conductivity was determined. However, the error associated with electrode drops is large only in the early afterglow, when the plasma impedance is less than the series resistance. It was checked by changing the series resistance in the probing pulse circuit, that a change of $\pm 50\%$ in this series resistance had no significant influence on the slope of the calculated electron density decay, and therefore the constant electrode drop assumption was sufficiently accurate bearing in mind other sources of errors e.g. determination of the discharge area.

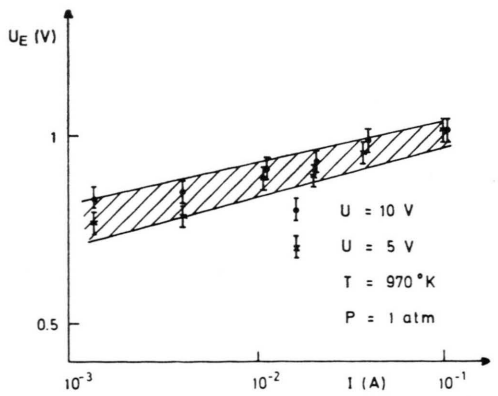

Fig. 5. Electrode drops as a function of probing current for two values of the probing e.m.f.

C) The Electron Density Decay

We made investigations in the temperature range from 600 – 970 °K and at pressures of 1, 2, 3 and 4 atm. Some experiments were also performed at higher pressures but they are not considered here, because the discharge was then not stable enough for reproducible measurements even at the highest temperature reached in this system.

The calculation of the conductivity was made straight-forwardly. The time dependent e.m.f. and the voltage across the electrodes were recorded on a Tektronix oscilloscope 556 with trimmed voltage probes. These results together with the spectroscopically measured area and the electrode drop were fed to a computer which evaluated the electron temperature, the conductivity and the axial electron density as a function of time.

The electron temperature, which enters into the calculation of the electron density, was derived from the energy equation taking into account joule heating and elastic losses. Heat conduction of the electrons may be neglected under the given conditions, and also radiation losses for the strongest visible lines. These latter were measured and found small in comparison with the elastic loss terms as pressures above 1 atm. The calculated electron temperature varied in the region between 1500 °K in

the early afterglow and 3000 °K in the late afterglow and hence was too small in order to contribute to thermal ionization in the afterglow. For a helium plasma dominated by neutral collisions the electron density is proportional to the square root of the electron temperature according to

$$n_e = \sigma_{eff} \cdot v_e \langle Q \rangle n_A m_e / e^2 . \quad (3)$$

v_e is the thermal velocity of the electrons, Q is the average momentum transfer cross-section at a given electron temperature, and n_A the density of the helium atoms. Since for helium $\langle Q \rangle$ is almost independent on T_e, the electron density depends only on $v_e \sim \sqrt{T_e}$ so that n_e is not too sensitive to an error of T_e. Anyhow, we tried also to measure the electron temperature directly by means of a Boltzmann plot of the excited atomic helium levels, but it was not possible to get a straight line even for the levels with the principal quantum number $n=6$ to $n=9$, the corresponding temperatures at a given condition in the early afterglow varying from 9000 °K for the levels $n=3$ and $n=4$ down to 2000 °K at the highest measured levels. A similar phenomena was found by Manalis [19] at low pressures in helium afterglows. There it was explained as an effect due to an electron gas with two different temperatures, the higher caused by superelastic heating of electrons in collisions with metastables.

Since at high pressures the relaxation time for the electron temperature is below 1 μsec, two electron temperatures are hardly to be expected in our case, instead dissociative recombination into excited lower atomic states as described by Stevefelt and Robben [9] could be a plausible explanation for the measured overpopulation of these levels. This would lead one to expect the correct electron temperature from the highest levels, corresponding to the lower limit of the electron temperature range mentioned above, which agrees quite well with calculated values.

D) Comparison between Electron Density and Light Intensity Decay

In Figure 6, the intensity decay for three different atomic lines is shown. There is a remarkable difference in the decay rates between the atomic helium and the ionic xenon lines on the one hand and the atomic xenon lines on the other hand. This holds for all observed strong lines of the respective excited species. Spectra taken at $t=100$ μsec in the afterglow exhibit only XeI lines, whereas those in the early afterglow are characterized by the variety of the XeI, XeII and HeI lines. Molecular bands were only very weak in the temperature and pressure range considered here.

The helium atomic light decays somewhat slower, when xenon is seeded to the gas. This behaviour is expected, because the main part of the upper 3^3D level is populated by recombining electrons and the intensity follows the relation

$$I(5876\,\text{Å}) \sim (n_e\,\text{He}^+)^a . \quad (4)$$

The experimental value of a is between 0.85 and 1. In the case of pure helium, n_e decays faster and therefore the line intensity should also do so. The XeII decay rates are somewhat smaller than those of He, but still much higher than those of XeI. Because even the ionic xenon lines with upper energy states close to that of the He(2^3S) metastable show the same behaviour, one has to conclude that the XeII lines are not governed by Penning processes. It is more likely that the excited Xe ions are produced during the active discharge and decay in the

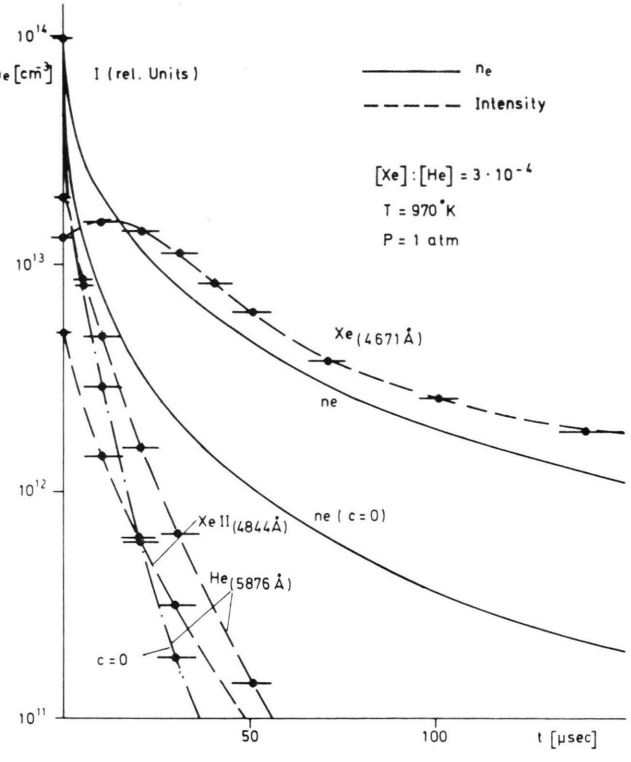

Fig. 6. Experimental decay of electron density and light intensity for pure helium ($c=0$) and a helium-xenon mixture with $c=3\cdot10^{-4}$. The bars indicate the sampling time.

early afterglow, leading to the observed fast decay of the XeII lines, which were only observable during the first 50 μsec.

In order to explain the measured slow decay of XeI lines in the late afterglow, an excitation process is required which involves directly the electron density in order to get $I(\mathrm{XeI}) \sim n_e$ as it follows from Figure 6, otherwise the xenon atomic lines in a recombining plasma should follow $I(\mathrm{XeI}) \sim n_e X_e^+ \approx n_e^2$. The fact that $I(\mathrm{XeI})$ is proportional to the electron density, as noted in Section III A, was also found from the XeI intensity profile scanned across the discharge at 50 μsec in the afterglow. One possible explanation may be the action of fast electrons which are created in superelastic collisions with metastables. Another explanation would be, that xenon atoms are ionized or excited via the following mechanisms

$$\left.\begin{matrix}\mathrm{He}^M + \mathrm{He} \\ \mathrm{He}_2{}^M\end{matrix}\right\} + \mathrm{Xe} \rightarrow 2\,\mathrm{He} + \begin{matrix}\mathrm{Xe}^+ + \mathrm{e} \\ \mathrm{Xe}^*\end{matrix} \qquad (5)$$

and hence Penning processes contribute to the similar slope of the decay curves of both XeI lines and the electron density. Anyhow, it is not possible at present to give more than a somewhat speculative explanation for this observation.

Instead we can describe qualitatively the experimentally observed decay rates of the electron density. Our xenon-seeded helium plasma consists mainly of the following important components: He and Xe atoms, He_2^+, Xe^+ and Xe_2^+ ions, metastable He^M or $He_2{}^M$, Xe^M and electrons (atomic He ions are converted into molecular ions in times below 1 μsec). In the active discharge, the electron temperature is about 8000 °K and the created plasma consists of comparable quantities of He_2^+ and Xe^+ ions, when the Xe-seed concentration is between 10^{-4} and 10^{-3}. After cessation of the main discharge pulse, both ion species decay according to the respective recombination coefficients. The recombination coefficients for both ion species are to be understood as effective recombination coefficients, because they include also source terms like metastable-metastable collisions and Penning processes. The effective recombination coefficient α_{eff} is defined by the rate equation for the electron density.

$$\begin{aligned} dn_e/dt &= -\alpha_{\mathrm{eff}}\, n_e{}^2 = -\alpha(\mathrm{He})\,\mathrm{He}_2{}^+ n_e - \alpha(\mathrm{Xe})\,\mathrm{Xe}^+ n_e \\ &\quad + \beta_{\mathrm{He}}(\mathrm{He}^M)^2 + \beta_{\mathrm{Xe}}(\mathrm{Xe}^M)^2 + k_p\,\mathrm{He}^M\,\mathrm{Xe} \\ &= -\alpha_{\mathrm{eff}}(\mathrm{He})\,\mathrm{He}_2{}^+ n_e - \alpha_{\mathrm{eff}}(\mathrm{Xe})\,\mathrm{Xe}^+ n_e \qquad (6) \end{aligned}$$

where $\alpha(\mathrm{He})$, $\alpha(\mathrm{Xe})$ denote the respective recombination coefficients, β_{He} the rate coefficient for the process $\mathrm{He}^M + \mathrm{He}^M \rightarrow \mathrm{He}_2{}^+ + \mathrm{e}$ (and analogously for Xe) and k_p the Penning ionization rate constant for the process according to $\mathrm{He}^M + \mathrm{Xe} \rightarrow \mathrm{Xe}^+ + \mathrm{He} + \mathrm{e}$. This latter process also acts as a coupling between the two decaying ion species. The observed n_e-decay follows then as a sum of the decaying Xe^+ and He^+ ions, the decay rate being dominated by the dominating species in any time. A plot of $1/n_e$ vs. time yields immediately the effective recombination coefficient from the inclination of the curve. This is shown in Figure 7 for the case with xenon

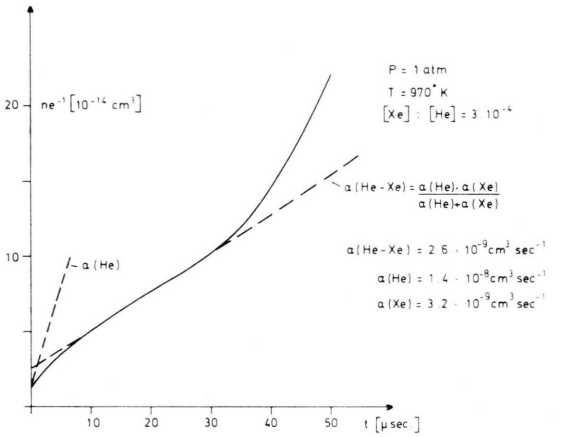

Fig. 7. $1/n_e$ vs. time for helium-xenon with $c = 3 \cdot 10^{-4}$ (α to be understood as an effective recombination coefficient).

seed. After a short fast increase, we have a nearly linear region up to about 30 μsec. From the fast increase at $t = 0$ one can deduce that He_2^+ must be the dominant ion in the early afterglow, but it decays at a higher rate than Xe^+. After about 10 μsec, Xe^+ is already dominant with a considerably lower decay rate. At large t, α_{eff} increases again, probably due to the fact that $\alpha_{\mathrm{eff}}(\mathrm{Xe})$ contains a source term which decreases in time. It is now possible to calculate the effective recombination coefficient $\alpha_{\mathrm{eff}}(\mathrm{He}-\mathrm{Xe})$ from the linear region of the curve in Figure 7. The following relation for the respective effective recombination coefficient holds at a time large enought $\left(t \gg \dfrac{1}{\alpha_{\mathrm{eff}}(\mathrm{He}-\mathrm{Xe}) \cdot n_e}\right)$:

$$\alpha_{\mathrm{eff}}(\mathrm{He}-\mathrm{Xe}) = \frac{\alpha_{\mathrm{eff}}(\mathrm{He}) \cdot \alpha_{\mathrm{eff}}(\mathrm{Xe})}{\alpha_{\mathrm{eff}}(\mathrm{He}) + \alpha_{\mathrm{eff}}(\mathrm{Xe})} \,. \qquad (7)$$

Under the assumption that $\alpha(\mathrm{He})$ is the same as for pure helium (from Figure 6 one can derive $\alpha_{\mathrm{eff}}(\mathrm{He})$

$= 1.4 \cdot 10^{-8}\,\mathrm{cm^3\,sec^{-1}}$ and $\alpha(\mathrm{He-Xe}) = 2.6 \cdot 10^{-9}$ $\mathrm{cm^3\,sec^{-1}}$) it follows than that $\alpha_{\mathrm{eff}}(\mathrm{Xe}) = 3.2 \cdot 10^{-9}$ $\mathrm{cm^3\,sec^{-1}}$. Furthermore, a computer fit of this curve gave the initial value for the He_2^+ ions as $7.7 \cdot 10^{13}$ $\mathrm{cm^{-3}}$ and that for Xe; as $2.3 \cdot 10^{13}\,\mathrm{cm^{-3}}$. (The time $t = 0$ was taken in all measurements at $n = 10^{14}$ $\mathrm{cm^{-3}}$ and that forXe^+; as $2.3 \cdot 10^{13}\,\mathrm{cm^{-3}}$. (The time $t = 0$ was taken in all measurements at $n_e = 10^4$ $\mathrm{cm^{-3}}$. The active discharge was adjusted so that the electron density for some t slightly less than zero, was slightly higher than this value.)

The relatively low decay rate for the xenon ions at a seed rate of $3 \cdot 10^{-4}$ may have a simple explanation: The partial pressure for xenon is so low, that molecular Xe-ions are not formed in appreciable amount during the investigated time interval of 150 μsec (the characteristic time for the formation of molecular Xe-ions under the given conditions is about 1 msec) and the recombination coefficient of atomic xenon ions is lower than that for molecular helium ions. It was shown by Johnson and Gerardo [6, 8] that He_2^+ ions undergo dissociative recombination to an appreciable extent with rates for $\alpha(\mathrm{He_2})$ in the order of some $10^{-8}\,\mathrm{cm^3\,sec^{-1}}$ depending on the pressure. Concerning the xenon ions, recombination coefficients for atomic xenon are not known to us, whereas $\alpha(\mathrm{Xe_2})$ was measured by Oskam and Mittelstadt [21] to be $1.4 \cdot 10^{-6}\,\mathrm{cm^3\,sec^{-1}}$. But the recombination behaviour of xenon can be assumed to be similar to that of argon, for which Biondi [22] showed that a He – Ar mixture of about 1‰ argon exhibits recombination coefficients of the order $10^{-9}\,\mathrm{cm^3\,sec^{-1}}$ compared with 10^{-6} $\mathrm{cm^3\,sec^{-1}}$ for pure (molecular) argon at the same total pressure. The latter high recombination rate was ascribed definitely to dissociative recombination. Hence analogously, the low recombination rates for atomic Xe^+ ions are not unexpected, and the measured effective value of $\alpha(\mathrm{Xe})$ $3.2 \cdot 10^{-9}$ $\mathrm{cm^3\,sec^{-1}}$ is reasonable. It is clear that in so far as Penning ionization plays an important role, it contributes to the low value of $\alpha(\mathrm{Xe})$.

It should be stated explicitly, that all the recombination coefficients given here represent only effective values as derived from the plasma resistivity and are rather to be used as equivalents for plasma decay times. Possible errors could originate from the uncertainty in the electron density profile, in the electron temperature and the electrode drops. However, confidence in the analysis is justified since the results fit throughout the picture of recombination behaviour established by other authors.

E) The Dependence of the Decay Rate on the Seed Concentration and the Pressure

When the model described above is correct, the decay rate should exhibit a minimum as the seed concentration monotonically increases from $c = 0$ to $c = 1$. This is clear from consideration of the limiting cases. For a given total pressure both pure molecular helium and pure molecular xenon ions exhibit higher decay rates. Only in the case, where the partial pressure of xenon is low enough and the ion conversion process

$$\mathrm{Xe^+ + Xe + He \xrightarrow{k_1} Xe_2^+ + He} \qquad (8)$$

is slow, can a decrease of the decay rate and α_{eff} be expected. The ion conversion coefficient k_1 was measured by Chen [23] to $1.1 \cdot 10^{-31}\,\mathrm{cm^3\,sec^{-1}}$. Hence the characteristic conversion time for the conditions at $P = 1$ atm, $T = 1000\,^{\circ}\mathrm{K}$ and $c = 3 \cdot 10^{-4}$ is ~ 1 msec and therefore larger than the time interval covered by the experiments. At seed concentrations higher than 10^{-3}, α_{eff} increases quickly as shown in Figure 8 and Xe_2^+ becomes the dominant ion during

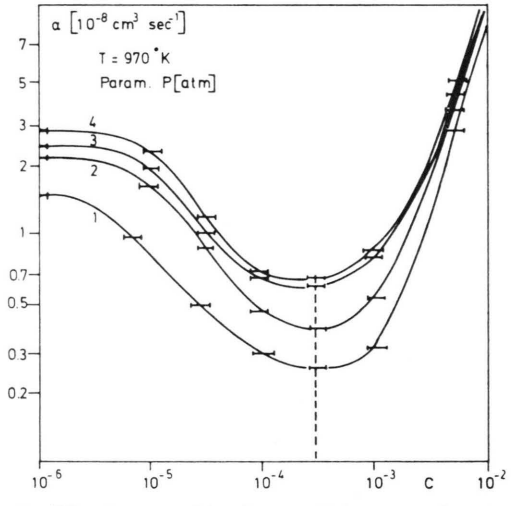

Fig. 8. Effective recombination coefficient as a function of the seed concentration for four different pressures. The values for $c = 10^{-6}$ agree with those for pure helium.

the total afterglow period. The minimum is flat and covers the region $10^{-4} < c < 10^{-3}$, and tends to move towards lower concentration, when the total pressures is raised, also in agreement with the model, because the increase of α_{eff} depends mainly

on the partial xenon pressure. In Figure 9, the results of the plasma decay behaviour at four different pressures are summarized. The curves represent the time dependence of $1/n_e$ for pure helium and optimum xenon seed (corresponding to the value indicated by a dashed line in Figure 8). A pressure dependence of the effective recombination coefficients

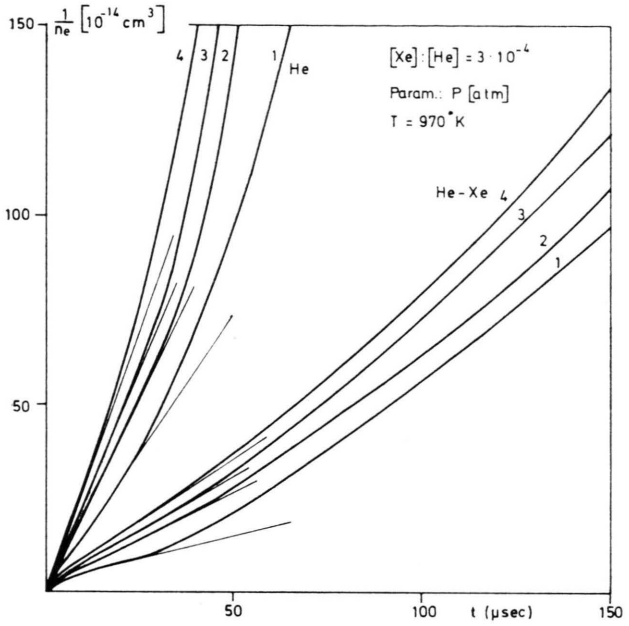

Fig. 9. $1/n_e$ vs. time for four different pressures at $T=$ 970 °K. Both cases with and without xenon seed are given.

is obvious, likewise the trend that α_{eff} increases in the later afterglow after $30-40$ μsec.

The pressure dependence for pure helium can be expressed as

$$\alpha_{eff}(\mathrm{He}) = \{(0.95+1.95\cdot10^{-3}P_0) \pm 0.15\}10^{-8}\,\mathrm{cm^3\,sec^{-1}} \qquad (9\,a)$$

where P_0 denotes the reduced pressure at $T=300$ °K in Torr. The indicated error only includes the deviation of the linear least mean square fit. (The total error was estimated to be of the order of $\pm 50\%$.) For helium-xenon mixtures, a linear fit leads to larger relative error for the chosen case of a constant seed concentration equal to $c=3\cdot10^{-4}$ and is given by

$$\alpha(\mathrm{He-Xe}) = \{(0.2=5.1\cdot10^{-4}P_0) \pm 0.06\}10^{-8}\,\mathrm{cm^3\,sec^{-1}}. \qquad (9\,b)$$

The ratio of the measured effective recombination coefficient without and with seeding decreases from 5.4 at 1 atm to 4 at 4 atm.

F) Temperature Dependence

The investigated temperature interval at $P=1$ atm was $600-970$ °K. At higher pressures we used generally the highest possible temperature in order to get a stable discharge. The temperature dependence was no longer as strong as found with the previous experimental system [15]. The measurements showed principally a decrease of the plasma decay rate with increasing temperature, when the pressure is kept constant. The found variation in α can be explained by the change in the reduced pressure and then described by the same Eqs. (9 a) and (9 b). However, these empirical formulas do not fit the temperature dependence of α well, as might be seen from the deviation of the experimental points from the dashed lines in Figure 10. The value of α_{eff} is

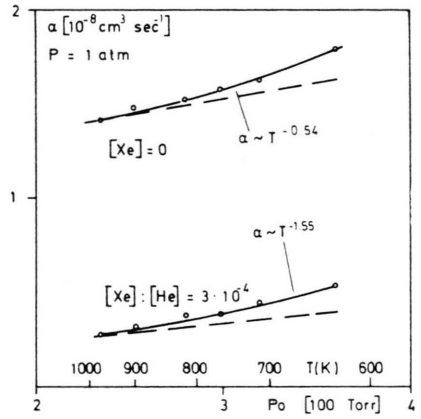

Fig. 10. Effective recombination coefficient with and without xenon seed as a function of the temperature, scaled as a function of the reduced pressure. The circles represent the experimental value, the dashed lines show the dependence as given by Eqs. (9 a) and (9 b), respectively. The full lines represent the respective temperature dependence.

not exactly a linear function of $1/T$, the recombination coefficient increases faster at lower temperatures compared with the formulae (9) describing the pressure dependence.

Thus it might be possible to regard the results as giving the variation of the dissociative recombination coefficient with the temperature. For pure helium, the plots in Figure 10 correspond to a temperature dependence.

$$\alpha \sim T^{-0.55} \qquad (10)$$

which is quite close to the value derived theoretically by O'Malley [24]. For the case that the molecular ions are in their ground vibrational state ($v=0$)

(which certainly holds for helium ions below 1000 °K), O'Malley [24] predicts an exponent of 0.5 for the temperature dependence.

For He – Xe mixtures, the temperature variation of α was found to be much stronger than the $1/t$ curve drawn in Figure 10. A logarithmic plot of these experimental data results in $\alpha \sim T^{-1.5}$ and could indicate dissociative recombination of molecular xenon ions in vibrationally excited states [24]. However, the low value of α makes dissociative recombination unlikely and the deviation from the Eq. (9 b) may be attributed to the temperature dependence of the atomic recombination coefficients, including loss and production terms of other interatomic processes (i.e. ion conversion and Penning ionization).

All the values reported above hold only for the early afterglow during the linear region in Figure 10 (max. 35 μsec) and during this time interval the calculated electron temperature was only slightly elevated.

Experiments with selective heating of the electrons by means of increasing the voltage of the probing pulse were not conclusive because no T_e measurements were performed in these series of experiments. Increasing the probing pulse e.m.f. from 5 to 10 Volt influenced the lifetime of our decaying plasma only slightly.

IV. Summary

The intention of this work has been to investigate the high pressure afterglow behaviour of a xenon-helium plasma, because such a plasma is of great interest for noble gas afterglow MHD generators. It was shown in a previous report [15] that by adding small amounts of another noble gas to helium the effective lifetime increases and that this effect is more marked with increasing atomic mass of the noble gas seed.

By seeding xenon to helium the effective recombination rates decreased remarkably. A minimum decay rate was found at seed concentrations of about $3 \cdot 10^{-4}$ for the investigated pressure range from 1 to 4 atm. For pure helium a pressure dependence of α corresponding to $0.95 + 1.95 \cdot 10^{-3} P_0) \cdot 10^{-8}\,\mathrm{cm}^3\,\mathrm{sec}^{-1}$ was found (1 – 4 atm), the relatively high absolute value attributed to dissociative recombination of molecular helium ions in the vibrational ground state ($v = 0$) because its temperature dependence of $\alpha \sim T^{-0.55}$.

For the He – Xe mixtures very low effective recombination coefficients were found which are explained by atomic xenon recombination at low seed rates. The intensity of atomic xenon lines followed fairly well the electron density decay during the first 150 μsec in the afterglow. The discharge was found to decay with two different decay rates: in the beginning faster according to the higher decay rates of excessive molecular helium ions, but slower after 10 – 15 μsec corresponding to a domination by the slower decaying atomic xenon ions. The pressure dependence in this case could be described by $\alpha_{\mathrm{eff}} = (0.2 + 5.1 \cdot 10^{-4} P_0) \cdot 10^{-8}\,\mathrm{cm}^3\,\mathrm{sec}^{-1}$, where P_0 is the reduced pressure at 300 °K. It is suggested that Penning ionization contributes to this low value of the effective recombination coefficient of atomic xenon.

When the optimum seed rate, where α_{eff} shows a minimum, was exceeded, the recombination coefficient increased steeply because of the enhanced production of molecular-xenon ions with a high recombination coefficient.

A discussion of these results in relation to the noble gas afterglow MHD generator is presented elsewhere [25].

Acknowledgements

The authors wish to express their gratitude do Dr. J. Braun for his stimulating interest and leadership, to Dr. S. Palmgren for many fruitful discussions during the course of the measurements and Dr. T. Robinson for discussion of the manuscript. We are also indebted to Mrs. G. Abrahamsson and Mr. S. Farvolden for invaluable assistance.

This work was performed with the financial support from the Swedish Board for Technical Development. By mutual agreement, a part of the experimental equipment was placed at our disposal by the Institut für Plasmaphysik, Garching, F.R.G. This is gratefully acknowledged.

[1] J. Braun, Plasma Physics **7**, 525 [1965].
[2] S. Palmgren, 1969, AB Atomenergi, Sweden (Internal report AE-FFA-848).
[3] D. R. Bates, A. E. Kingston, and R. W. P. McWhirter, Proc. Roy. Soc. London **A 267**, 297 [1962], and Proc. Roy. Soc. London **A 270**, 155 [1962].
[4] J. Berlande, M. Cheret, R. Deloche, A. Gonfalone, and C. Manus, Phys. Rev. A **1**, 887 [1970].
[5] J. Stevefelt, J. Phys. D **4**, 899 [1971].
[6] A. W. Johnson and J. B. Gerardo, Phys. Rev. A **5**, 1410 [1972].

[7] D. R. Bates and S. P. Khare, Proc. Roy. Soc. London **85**, 231 [1965].
[8] A. W. Johnson and J. B. Berardo, Phys. Rev. Lett. **28** 1096 [1972].
[9] J. Stevefelt and F. Robben, Phys. Rev. A **5**, 1502 [1972].
[10] F. Robben, Phys. Rev. A **5**, 1516 [1972].
[11] M. A. Gusinov, R. A. Gerber, and J. B. Gerardo, Phys. Rev. Letters **25**, 1248 [1970].
[12] J. B. Gerardo and M. A. Gusinov, Phys. Rev. A **3**, 255 [1971].
[13] I. Ya. Fugol, V. M. Samovarov, and M. G. Starkov, J. Exp. Theor. Phys. **60**, 1637 [1971].
[14] W. H. Ellis, K. Imani, and S. H. Kim, Proc. Vth Int. Conf. on MHD Electr. Power Generation, Munich, **II**, 21 [1971]. and **IV**, 27 [1971].
[15] H. Zinko, J. Stevefelt, and J. Johansson, Proc. Vth Int. Conf. on MHD Electr. Power Generation, Munich, **II**, 25 [1971].
[16] G. Hahn and G. Salvat, Proc. Vth Int. Conf. on MHD Electr. Power Generation, Munich, **II**, 11 [1971].
[17] E. P. Gray and D. E. Kerr, Ann. Phys. **17**, 276 [1962].
[18] H. Zinko, Unpublished calculations.
[19] M. S. Manalis, Phys. Rev. A **4**, 364 [1971].
[20] A. W. Johnson and J. B. Gerardo, Phys. Rev. A **5**, 1410 [1972].
[21] H. I. Oskam and V. R. Mittelstadt, Phys. Rev. **132**, 1445 [1963].
[22] M. A. Biondi, Phys. Rev. **83**, 1078 [1951].
[23] C. L. Chen, Pyhs. Rev. **131**, 2550 [1963].
[24] Th. O'Malley, Phys. Rev. **185**, 101 [1969].
[25] H. Zinko, AB Atomenergi, report in preparation.